Granular Matter (2024) 26:47
https://doi.org/10.1007/s10035-024-01419-1

ORIGINAL REPORT

# A study of membrane correction accounting for both curvature and tension in DEM simulations of triaxial tests of sand and ballast with two alternative flexible membrane models

**Mathias Tolomeo**[1] · **Glenn R. McDowell**[1]

Received: 28 September 2023 / Accepted: 29 February 2024


**Abstract**
In DEM simulations of triaxial tests, modelling a flexible lateral membrane is crucial and challenging. It is essential for the correct application of a uniform lateral pressure and for an accurate measurement of sample volume. Here, we introduce a membrane made of triangular facets, and model it as a continuum; we then compare this approach with a well-established method that uses a layer of bonded spheres. With either method, it is also possible to assess the additional stress applied by the membrane as it deforms, i.e. the difference between the stress applied at the boundary and the actual stress within the sample. It is shown that this difference has two origins: the tension developed in the membrane, as it deforms; and the curvature of the membrane, since this causes a vertical component of the confining pressure which can be significant. These findings may be used to inform and improve the membrane correction commonly used in experiments, where similar effects occur.

**Keywords** Discrete Element Method · Flexible membrane · Triaxial test · Membrane correction · Sand · Railway ballast

## 1 Introduction

In the DEM modelling of triaxial tests on soil, one of the most important features and challenging tasks is the modelling of a flexible membrane. This is crucial in order to achieve realistic behaviour of the material. The main purpose for using a flexible lateral boundary in laboratory triaxial tests is to limit the lateral constraint on the sample, while applying a vertical load, so that the sample remains quite free to deform as it naturally would in the lateral direction. By doing so, it can be assumed that the natural failure mode can develop. However such membranes are known to have an effect on the stress within a sample [1, 2].

In DEM, a properly modelled flexible membrane allows for lateral pressure, applied by a confining fluid, to be applied uniformly over all regions of the lateral surface, as well as for volumetric deformations to be measured accurately. A rigid cylindrical boundary would instead result in stress concentrations, and would also prevent any strain localisation from taking place.

In early DEM work on 3D triaxial tests, true triaxial conditions, i.e. cubical samples with flat rigid boundaries, were often used [3, 4], instead of replicating the axisymmetric conditions of a standard triaxial test, for which a cylindrical flexible membrane was needed. Some early attempts at modelling a flexible membrane in 3D included the application of lateral forces directly onto sample grains [5].

Other methods model the membrane as a separate body, e.g. as a layer of bonded monodisperse spheres ([6–9] among others) or as a set of connected triangular facets with degrees of freedom in their vertices [10, 11]. The former approach, in particular, has recently become quite popular, as it is simple to implement and has been proven to work effectively. Among other applications, this allowed for a realistic modelling of the very heterogeneous lateral deformation of a railway ballast triaxial sample [7, 12].

Despite its success, this approach also has some limitations. In particular, the choice of bond parameters, despite some attempts at linking them to the membrane material properties, still remains rather arbitrary. Other parameters that can affect the response include the resolution adopted (i.e. the size and number of spheres), the geometrical arrangement of spheres, and their initial overlap. A sufficient

✉ Mathias Tolomeo
mathias.tolomeo1@nottingham.ac.uk

[1] Nottingham Centre for Geomechanics, University of Nottingham, Nottingham NG7 2RD, UK

Published online: 25 March 2024

resolution, in particular, is required in order to have a membrane that is as continuous as possible and avoid gaps, which may however still occur, considering its discrete nature, especially at large strains and when the sample dilates. Spheres should therefore be small enough to prevent the smallest grains from escaping; this can lead to membranes made of a very large number of small spheres, and can also reduce the simulation timestep. Both these will impact the computational performance.

Due to these limitations, it can be worth considering alternative ways of modelling a flexible membrane. A faceted membrane, with triangular facets connected to each other, whose vertices can move independently, can solve most of the bonded spheres membrane limitations. In particular, it provides geometric continuity with no need to resort to impractically high resolutions. In order to achieve a realistic response, it is important to include realistic material properties in the modelling of the deformation of such a membrane.

Independently of the method used for modelling the membrane in DEM, it is important to acknowledge that there is an effect of the membrane on the internal state of stress of the sample, just like in experiments. In DEM, this effect comes from the same causes that act in experiments; however, in case there should be any additional effect due to specific features of the DEM model, this needs to be acknowledged. It is therefore important to achieve a membrane model that is as realistic as possible, and that does not add any unwanted/unphysical effect on the internal stress. Membrane effect has been often overlooked in previous DEM works, but it is an important feature that should not be neglected. In DEM it is possible to measure the internal state of stress directly from the interparticle contact forces, thus allowing for a simple estimation of membrane effect as a result of the comparison with the external stress that is measured at the boundaries, in a similar way to the measurements obtained experimentally.

In the following sections, after describing the two different membrane models adopted, the approach to the estimation of membrane effect will be described, highlighting all stress components involved. The insights obtained with this approach may also be useful for experiments: some of the corrections to external stress highlighted here also apply to the experimental case, and could be used to inform and improve the corrections currently adopted by the specifications.

## 2 Modelling a flexible membrane in DEM

### 2.1 Faceted membrane

The faceted membrane adopted here is obtained by defining a hexagonal arrangement of points on the sample's lateral surface. The edges connecting neighbouring nodes define triangular facets. Each node can move independently of the others, which makes this membrane flexible.

The commercial software used for the DEM simulations is PFC3D [13], and it can be used in combination with the finite-volume code FLAC3D [14], thus providing a solution for continuum modelling of the membrane based on its real material properties.

The membrane is modelled here as a shell structure resisting only membrane action (no bending action). Each triangular facet defines one shell element. Each element is modelled as a thin-shell constant strain triangle (CST) element, for which transverse shear deformations can be neglected. Elements are assumed to follow the behaviour of an isotropic, linearly elastic material; the parameters defined for the constitutive model are Young's modulus $E = 1.4$ MPa and Poisson's ratio $\nu = 0.3$. Membrane thickness also needs to be assigned; depending on the type of laboratory test to be simulated, different values can be chosen—e.g. a thicker membrane for ballast compared to sand. The two end rows of the faceted membrane are rigidly attached to the polyhedral elements that are used to simulate the end platens in the DEM model (Fig. 1c).

### 2.2 Bonded spheres membrane

Bonded spheres membranes have become increasingly popular in recent years [6–9]. All applications are quite similar to each other. Some differences can be found in the geometry, e.g. in the resolution (number and size of spheres) as well as in the geometrical arrangement: most applications use a hexagonal arrangement, though a square one can also be found [15].

Bond stiffness parameters can affect the response of the membrane, and should therefore be chosen with care.

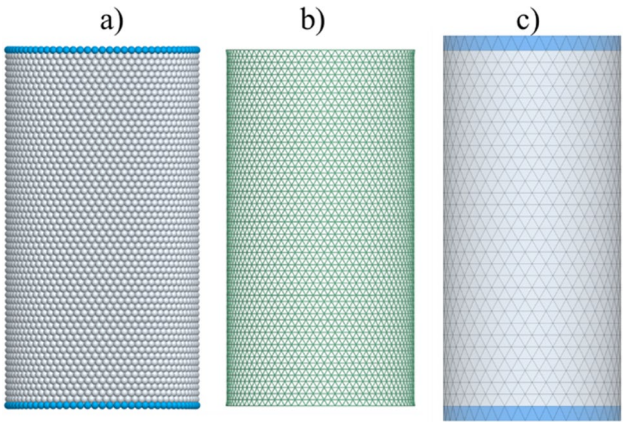


**Fig. 1** Image of two different DEM models of a flexible membrane: **a** layer of bonded spheres; **b** corresponding network of bonds; and **c** faceted membrane

Some authors have proposed an approach to match results of experimental tests on membranes without the granular material [7], while others used a calibration based on strain energy that links the microscopic stiffness parameters with the membrane's macroscopic properties [16, 17]. Using this approach, bond stiffnesses in the normal and tangential direction were determined also in this work as a function of the same macroscopic properties adopted for the faceted membrane in Sect. 2.1 (Young's modulus $E$, Poisson's ratio $\nu$ and membrane thickness $t$), based on the following equations:

$$\begin{cases} k_n = \frac{Et}{\sqrt{3}(1-\nu)} \\ k_s = \frac{Et(1-3\nu)}{\sqrt{3}(1-\nu^2)} \end{cases} \tag{1}$$

Spheres can sometimes be slightly enlarged so that they initially overlap, to remove gaps and improve continuity; however, this may increase the possibility of contacts between non-neighbouring spheres, which, being compressive, may generate unwanted deformation patterns. Therefore, here spheres were generated with no initial overlap.

## 3 Estimating the membrane effect

The effect of such membrane models on the stress within a sample has rarely attracted much attention. De Bono et al. [8] acknowledged and compensated for a membrane effect by enlarging spheres as the membrane deforms, to relieve excessive radial stresses. Le Pen et al. [18] tried investigating this effect with simple DEM simulations of spheres in a face centred cubic packing, modelling the membrane as an array of points surrounding the specimen and connected elastically.

More recently, Huang et al. [17] analysed membrane effect by looking at the change in stress as a result of a change in bond stiffness parameters, although without resorting to stress computations from interparticle forces which can shed more light on how the membrane affects stress.

In experiments, membrane effect is typically estimated and corrected by assuming the membrane deforms as a right-cylinder, or by resorting to compression shell theory (when the membrane follows the deformation of the specimen) and hoop tension theory (if the membrane buckles) [1, 2]. However, these situations do not always capture the membrane's behaviour realistically, especially when the membrane deformation is highly heterogeneous. This can come e.g. from strain localisation, but particular deformation patterns can also appear when the membrane tends to penetrate through large pores, e.g. when particles are relatively large compared to the sample such as for tests on railway ballast.

### 3.1 Stress tensor from boundary or internal forces

Nicot et al. [19] give the following definition of the average Cauchy stress tensor in a granular assembly, based on the classic Love-Weber formula [20–22]:

$$\langle \sigma_{ij} \rangle_{LW} = \frac{1}{V} \sum_{p \in \partial V} f_i^{ext,p} x_j^p = \frac{1}{V} \sum_{p \in \partial V} f_i^{ext,p} x_j^{G_p} + \frac{1}{V} \sum_{p \in \partial V} f_i^{ext,p} r_j^p, \tag{2}$$

where external forces $\vec{f}^{ext,p}$ on the boundary $\partial V$ are applied at contact points of position $\vec{x}^p$ and are acting on boundary particles of position $\vec{x}^{G_p} = \vec{x}^p - \vec{r}^p$ (Fig. 2). When the number of particles in a sample is sufficiently large, $\|\vec{r}^p\| \ll \|\vec{x}^{G_p}\|$ and therefore the second term can be omitted.

This expression defines the stress tensor as a function of external forces, but a perfectly equivalent expression can be derived from Eq. 2, having omitted the second term, using interparticle contact forces instead of external forces [19]:

$$\langle \sigma_{ij} \rangle_{LW} = \frac{1}{V} \sum_{c=1}^{N_c} f_i^c l_j^c + \frac{1}{V} \sum_{p \in V} \left( f_i^p - w_i^p \right) x_j^{G_p}, \tag{3}$$

where $\vec{f}^c$ and $\vec{l}^c$ are the contact force and branch vector (connecting the two particles' centres of mass) for each interparticle contact $c$, while $\vec{f}^p$ and $\vec{w}^p$ are the resultant and gravitational force acting on each particle $p$. Gravity has not been modelled in the DEM simulations carried out in this work, therefore $\vec{w}^p$ will be henceforth omitted.

### 3.2 Membrane considered as external to the sample

Considering the sample as composed only of its particles, and combining Eqs. 2 and 3 to calculate the stress tensor from external and internal forces, the following expression holds:

$$\frac{1}{V} \left( \sum f_i^{(1)} x_j^{(1)} + \sum f_i^{(2)} x_j^{(2)} \right) = \frac{1}{V} \left( \sum f_i^{(3)} l_j^{(3)} + \sum f_i^{(res.)} x_j^{(res.)} \right), \tag{4}$$

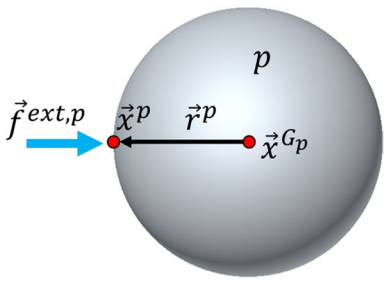


**Fig. 2** Centre and point of application of the external force on a membrane sphere

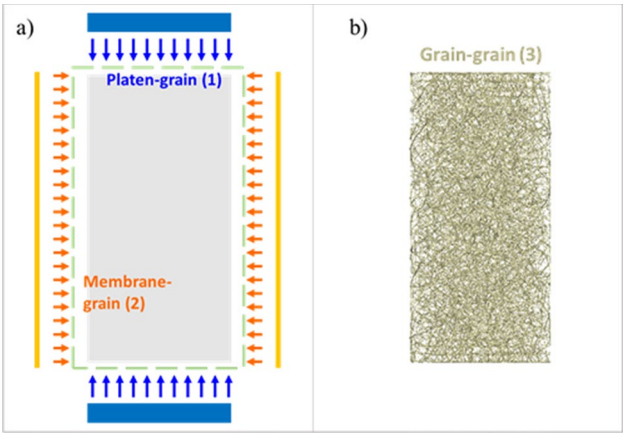


**Fig. 3** Image showing the groups of forces used to define each stress tensor in Eq. 4, with the membrane considered as external to the sample: **a** external forces applied to the sample; **b** internal forces of the sample

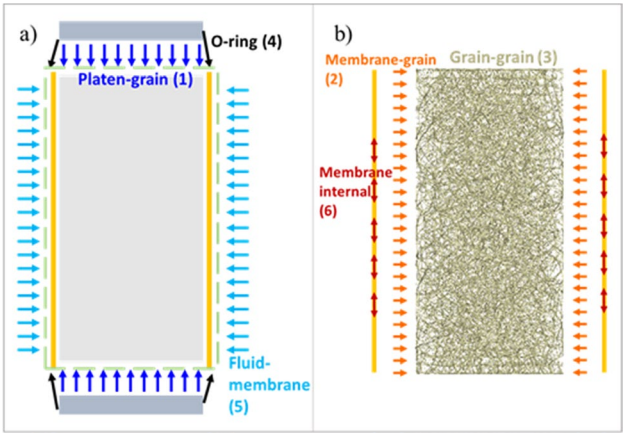


**Fig. 4** Image showing the groups of forces used to define each stress tensor in Eq. 5, with the membrane considered as part of the sample: **a** external forces applied to the sample and membrane; **b** internal forces of the sample + membrane system

with each stress tensor obtained from a different group of forces, marked with a different number, as indicated in Fig. 3. In particular, the left hand-side is obtained from Eq. 2 considering forces applied by the platens (1) and the membrane (2) to the grains, while the right-hand side comes from Eq. 3, considering grain-to-grain contacts (3) and resultant forces of grains (having omitted gravity). Stress tensors from external forces are calculated using contact positions $\vec{x}^{(n)}$, as in the general form of the equation (Eq. 2), while stress tensors from internal forces use branch vectors $\vec{l}^{(n)}$, as in Eq. 3.

### 3.3 Membrane considered as part of the sample

If we consider the membrane as part of the sample, it is possible to calculate a stress tensor of the whole system composed of the grains and the membrane. By doing so, we can obtain an expression equivalent to Eq. 4, and compare the two expressions to highlight the difference between the stress applied to the membrane and the stress that is actually transmitted to, and felt by, the grains within the sample.

The groups of forces identified as external and internal under this assumption are shown in Fig. 4. External forces, to be used in Eq. 2, are now the forces applied by the platens to the grains (as in Sect. 3.2) and the forces applied by the confining fluid to the membrane (instead of the forces transmitted by the membrane to the grains, that were used in Sect. 3.2). In the case of faceted membrane, the confining pressure applied is equivalent to a set of forces that are each acting on one triangular facet of the membrane, in a direction normal to the facet, and with magnitude equal to the facet's area multiplied by the confining pressure; a similar set of forces can be identified for the bonded spheres membrane. In addition, the forces exerted by the platens onto the membrane to fix its position at the two ends should be included here; this will be referred to as "O-ring forces" as they correspond to the sealing action performed by O-rings in a laboratory test setup. In the case of a bonded spheres membrane, these O-ring forces can be determined as the resultant forces acting on the two layers of spheres that are fixed to the platens and follow their motion. For the faceted membrane, such forces are determined in a similar way, as the resultant forces on those membrane nodes that are connected with the platens and fixed to their position.

The internal forces to be used in Eq. 3 will now include, in addition to the interparticle contact forces and resultant forces on grains, the internal forces acting within the membrane, as well as the resultant forces acting on membrane elements. For the bonded spheres membrane, these forces will be respectively the contact forces acting at each bond between membrane spheres and the resultant forces on each sphere. For the faceted membrane, equivalent forces can be identified in a similar way, based on the data returned by the software: a "contact" force will be the force between each facet's centroid and the facet's three vertices, while resultant forces are directly provided at each facet's centroid.

Having defined external and internal forces in this way, the combination of Eqs. 2 and 3 gives:

$$\frac{1}{V}\left(\sum f_i^{(1)} x_j^{(1)} + \sum f_i^{(4)} x_j^{(4)} + \sum f_i^{(5)} x_j^{(5)}\right) = \frac{1}{V}\left(\sum f_i^{(3)} l_j^{(3)} + \sum f_i^{(6)} l_j^{(6)} + \sum f_i^{(2)} l_j^{(2)} + \sum f_i^{(res,p)} x_j^{(p)} + \sum f_i^{(res,m)} x_j^{(m)}\right) \quad (5)$$

Each group of forces is identified with a number as indicated in Fig. 4; the last two elements take into account unbalanced forces on grains and membrane nodes.

By solving Eqs. 4 and 5 for the common term containing interparticle contact forces $\frac{1}{V}\sum f_i^{(3)} l_j^{(3)}$, it is possible to

obtain an expression linking the stress applied by the cell fluid to the membrane with the stress actually transferred by the membrane to the sample:

$$\frac{1}{V}\left(\sum f_i^{(2)} x_j^{(2)} - \sum f_i^{(5)} x_j^{(5)}\right) = \frac{1}{V}\left(\sum f_i^{(4)} x_j^{(4)} - \sum f_i^{(6)} l_j^{(6)} - \sum f_i^{(2)} l_j^{(2)} - \sum f_i^{(res.,m)} x_j^{(m)}\right) \quad (6)$$

The left-hand side of Eq. 6 is the difference between the lateral stress transferred to the sample (2) and the lateral stress applied to the membrane (5); the terms on the right-hand side are, respectively, the stress due to O-ring forces (4), the stress due to membrane internal forces (6), a stress correction that accounts for the transfer from the point of application of lateral forces (2) to the centre of boundary particles, and the stress due to unbalanced forces in the membrane (which can be neglected if the simulation is carried out with a sufficiently low strain rate, i.e. 1 or 2 orders below the limit of quasi-static behaviour [23]). Also the term $\sum f_i^{(2)} l_j^{(2)}$ can be assumed to be small compared to the other terms, and neglected, if the particles are sufficiently small, for the same argument used in Eq. 2 to discard the term with $\vec{r}^p$. This term was indeed found to be very small in the tests shown here (< 1 kPa for simulations at 60 kPa). In typical soil samples (e.g. sand), with much smaller particles, this term would be even smaller, so it is safe to neglect it. It is then clear that the difference between the stress applied laterally and the actual stress within the sample is a function of both the stresses developed inside the membrane as it deforms and the forces that fix the position of the membrane at the two end platens. These need to be considered when correcting the stress tensor calculated from external forces.

### 3.4 Geometric effect of membrane deformation: axial component of confining pressure

In triaxial tests, and in DEM simulations of such tests, it is typically assumed that the lateral (radial) stress is applied uniformly and remains constant throughout the whole test, while the axial stress changes as a deviatoric strain is applied, and it is measured from contact forces at the end platens. It was shown in Sect. 3.3 that the stress transmitted laterally differs from the one actually applied, due to stresses within the membrane and at the contact between the membrane and the end platens, both of which can be estimated in DEM simulations.

However, another source of error—possibly the main one, and often overlooked in both simulations and experiments—comes from considering the stress applied to be constant. This assumes that the sample preserves its original cylindrical shape as it deforms throughout the test. While this can be a convenient assumption (e.g. for estimating a radial deformation from the measured axial and volumetric deformation), it can also be very far from reality, especially when relatively large deformations are achieved. In general, as the sample and membrane deform, there are two most common situations: if the deformation remains uniform, the sample often expands radially and normally bulges, especially when the response is dilative, with the largest expansion happening around the middle section, while the deformation near the two ends is smaller due to the membrane being constrained to follow the platens; if, on the other hand, strain localises around a shear band, the radial deformation may be less predictable as the sample becomes segregated by the shear band in two (or more) blocks displacing almost rigidly, separated by a thin layer of dilating soil. Here, we will focus on the first situation. The deviation from the cylindrical shape is a function of the radial strain, which means that the deviation increases with the tendency of a sample to dilate as it is sheared.

The confining pressure is applied normally to the membrane surface; due to this deviation from the cylindrical shape, at large strains the confining pressure in general is no longer acting only in the radial direction, but it develops forces in the axial direction as well. This applies also to the case in which the deviation from the cylindrical shape happens because of an overall decrease in volume of the sample; its effect may therefore be compressive or tensile depending on whether the sample has expanded or contracted in the radial direction (Fig. 5). In case of radial shortening, the global contribution of the confining pressure in the axial (vertical) direction is equivalent to the effect of forces pulling the two end platens apart, i.e. it is a tensile contribution ($\sigma_{zz,app} < 0$). If the sample expands radially, the overall contribution is a compressive one ($\sigma_{zz,app} > 0$), adding on to the compression applied by the platens. This situation, in particular, should be treated with care, as the deviation from the undeformed shape can be more significant in this case, and therefore the contribution can be significant comparing with the axial stress transmitted through the platens. Hence, this should be considered when correcting stress measurements in DEM simulations, and it might be significant also in laboratory tests. On the other hand, the geometric effect of membrane deformation has no effect on the radial components of the laterally applied stress, which have been verified to remain constant and equal to the confining pressure applied even when the membrane has deformed.

## 4 Results: membrane effect broken down in its components

### 4.1 Sample generation and properties

DEM simulations of triaxial tests were carried out by means of the popular commercial software PFC3D [13]; two different samples were used (Fig. 6). A quite dense sample of coarse sandy material (h = 76 mm, d = 38 mm) was generated with 25,000 grains, using a library of 14 irregular shapes. These shapes had been previously obtained from laser scans of railway ballast grains, and it is assumed they can be used to reproduce a realistic sample of angular sand. Polyhedral blocks, with about 100 faces each, were used to model each particle's shape; these proved to be more computationally efficient than clumps (clusters of overlapping spheres) with such a large number of particles. The particle size distribution has a $d_{50}$ of 1.7 mm and a uniformity coefficient $C_u$ of 1.34. A membrane thickness of 0.3 mm is assumed for this sample for both models used. Grains were first generated with a smaller size, and then expanded until a void ratio $e_0 = 0.6$ was achieved.

The second sample analysed is a large triaxial sample of railway ballast (h = 450 mm, d = 300 mm) obtained from X-Ray scans of an untested laboratory sample subject to resin impregnation [12]. In this case, clumps were used to model particle shape; this was possible due to the relatively small number of particles, which also allowed for a higher resolution for each particle (about 100 spheres per particle). Clumps have been shown to capture some aspects of the mechanical response of ballast better than equivalent polyhedra [24]. A much thicker membrane is used in laboratory tests on ballast, to avoid piercing; a thickness of 4 mm was chosen for the simulations, as in previous experimental tests on similar samples.

A classic Hertz contact model was used, with $E = 70$ GPa and $\nu = 0.2$ for both materials; a higher Young's modulus (210 GPa) was assigned to the steel end platens. An interparticle friction coefficient $\mu = 0.6$ was used for ballast,

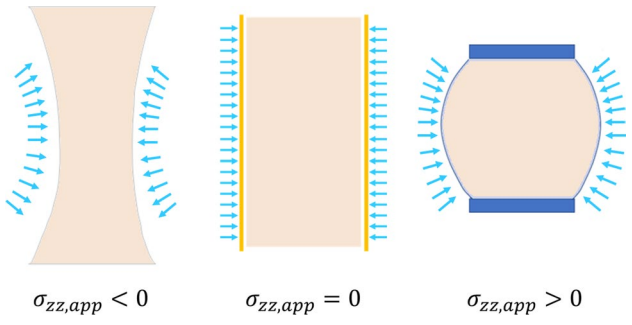


**Fig. 5** Image describing the orientation of the lateral confining pressure as a function of the sample's radial deformation: contraction (left), no deformation (centre) and expansion (right)

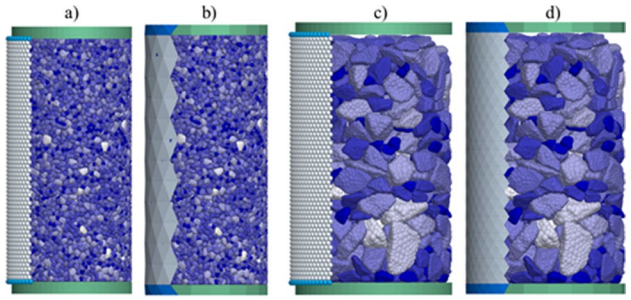


**Fig. 6** Image of the two samples used in DEM simulations with both membrane models: **a** and **b** coarse sand (h = 76 mm, d = 38 mm) modelled with polyhedral blocks; **c** and **d** large triaxial sample of railway ballast reconstructed from X-Ray CT scans (h = 450 mm, d = 300 mm), modelled with clumps. Particles are colourised based on their volume, with different scales for the two samples (color figure online)

and $\mu = 0.2$ for sand, consistently with data from experimental interparticle tests by [25, 26] respectively. For both membrane models, the contact parameters assigned to the membrane were the same as those used for modelling the membrane's behaviour, i.e. $E = 1.4$ MPa and $\nu = 0.3$. Both membranes and platens were assumed to be frictionless. For the bonded spheres membrane, bond stiffness parameters were determined based on Eq. 1 using the same membrane properties $E$ and $\nu$, as well as the appropriate membrane thickness $t$ for each case.

A hexagonal geometrical arrangement was used for both membrane models. The faceted membrane for the sand sample is composed of 480 triangular facets (12 layers); two additional layers were added in correspondence of the end platens and are attached to them, to mimic the effect of O-rings in laboratory tests (Fig. 1c). As long as the membrane deformation profile is expected to be smooth (when the number of grains is sufficiently high), a higher resolution is not normally required, as this model already provides geometrical continuity (no holes). However that is not the case for ballast, for which membrane deformation is known to be very irregular due to the large size of grains and pores, and therefore a higher resolution (2400 facets, 30 layers) was used. On the other hand, a higher resolution is always needed for the bonded spheres membrane, since this is also related to the size of the spheres used, which should be small enough to provide a realistic deformation (preventing large overlaps between membrane spheres as they move) and to avoid large gaps which would allow small grains to exit the sample. A set of 4800 spheres with a radius of 0.8 mm for the sand sample, and 8400 4 mm spheres for the ballast sample, were found to satisfy these two criteria; these include two layers (one at each end) that are attached to the end

platens, in a similar way to the other model (Fig. 1a). Figure 7 shows the deformation of both membranes at the end of shearing ($\varepsilon_a = 30\%$) in simulations of sand.

Before shearing, each simulation starts with a phase of isotropic consolidation, where a confining pressure is applied, with a gradual increase up to the target value, to the membrane and top platen simultaneously, while the bottom platen is not allowed to move. In simulations of the sand sample, the top platen was prevented from rotating, while it was allowed to rotate for the ballast samples, to replicate the laboratory conditions of those tests. Both membrane models managed to handle the deformation, while still preserving the attachment condition at the two ends, including in the case of the rotating top platen. No gravity was modelled in any of these simulations. However, it is not expected that it would affect the results significantly; also, it would be easy to account for it in the calculation of stresses from Eq. 3.

After an equilibrium state was achieved at the end of isotropic consolidation, shearing was applied by assigning a constant vertical upwards velocity to the bottom platen, while preventing the top platen from displacing (only rotation was allowed in the simulations of ballast). The shear rate applied had to be sufficiently low in order to reduce unwanted inertial effects and be able to apply the definition of Love-Weber stress tensor in Eq. 2 and all following equations derived from it. To demonstrate this, the strain rate had to comply to the condition on the inertial number $I = \dot{\varepsilon}\sqrt{\frac{m}{pd^{D-2}}} < 10^{-3}$ [23], where $I$ is a function of strain rate, pressure, grain size and mass. Velocities of 0.1 m/s and 0.01 m/s were therefore chosen for the sand and ballast simulations, respectively.

Figure 8 shows the stress–strain and volumetric response for simulations of sand using the two different models. Stress components were calculated from internal forces, as in Eq. 3. The behaviour is similar between the two models, and it captures the main features of dense sand behaviour: peak and critical state happen at the same axial strain for both simulations; the peak in shear stress matches well the highest dilation; the friction angle at zero dilation is essentially the same as the critical state friction angle. Therefore it can be concluded that both models can be successfully used. While the faceted model seems generally preferable, for the reasons presented in Sect. 2, they both provide satisfactory results and therefore both will be used in the analysis of membrane effect in the following sections, also to investigate if they have a different effect on the stress state within a sample.

## 4.2 Membrane effect and correction of radial stress

Having computed all stress tensors as explained in Sect. 3, it is possible to break stress down into distinct components and highlight the effect of the membrane on stress.

Figure 9 shows the evolution of membrane radial stress in a simulation of sand with bonded spheres membrane. Radial stress is computed as the sum of stress components in the radial direction due to membrane internal forces and to link forces between membrane and platens (O-ring forces). Figure 9 also shows that this stress is equal to the difference between the radial stress applied externally (constant and equal to the applied confining pressure, as was verified by computing it from the forces applied onto each facet/sphere) and the radial stress transmitted to the sample (calculated from contacts between membrane and grains), as demonstrated by Eq. 6. The comparison of Fig. 9a with b shows that the magnitude of the membrane radial stress typically increases with the stress level.

It can be observed that membrane radial stress can take both negative and positive values; here, it starts as negative and then quickly increases and becomes positive (compressive). An initially negative membrane radial stress means that the membrane can also take on some of the applied pressure, i.e., the pressure transferred to the sample can be lower than the applied pressure. After the initial contraction, as the sample dilates, the membrane radial stress will increase and eventually turn positive, meaning that it will add on to the applied pressure. The rate of increase reaches a maximum value, after which it slows down, until radial stress reaches a plateau. This behaviour seems more consistent with the volumetric behaviour, rather than with the radial strain that increases monotonically even at large strains, and this is confirmed by drawing the two curves together (volumetric strain and radial stress, Fig. 10). The curves look very similar from a qualitative point of view, and, most importantly, there is a good match between the point of maximum rate of increase of both volumetric strain (i.e. dilation) and radial stress, as well as between the point of zero volumetric strain and that of zero radial stress. The dependence of membrane radial

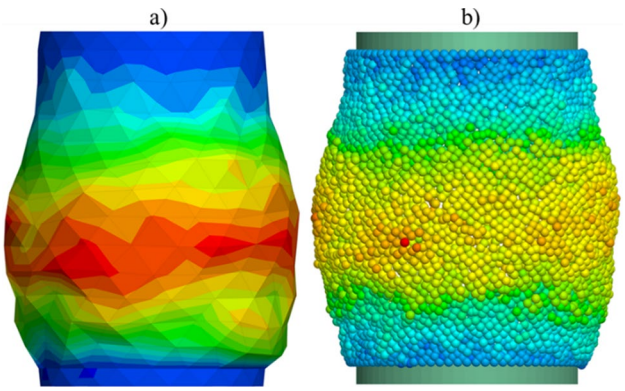


**Fig. 7** Membrane deformation for an axial strain of 30%, for a faceted (left) and bonded spheres (right) membrane, in DEM simulations of sand. Colourisation is based on the distance from the sample's axis (radial coordinate) (color figure online)

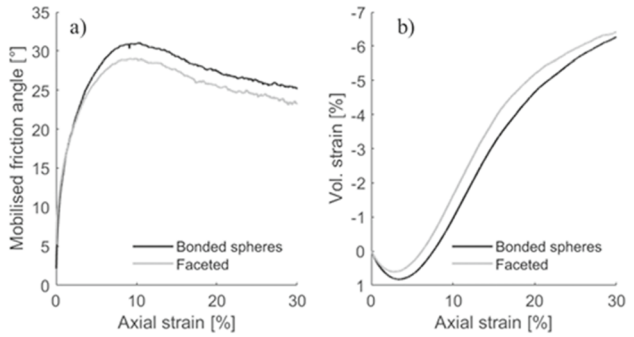


**Fig. 8** **a** Stress–strain and **b** volumetric response of DEM simulations of sand with the two membrane models, for a confining pressure of 60 kPa

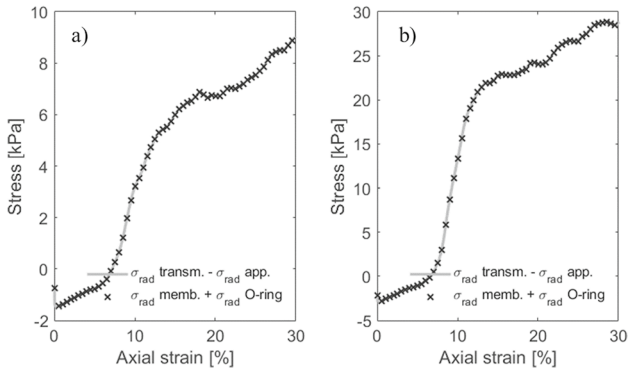


**Fig. 9** Evolution of membrane radial stress in DEM simulations of sand using a bonded membrane, with **a** 60 kPa and **b** 300 kPa confining pressure

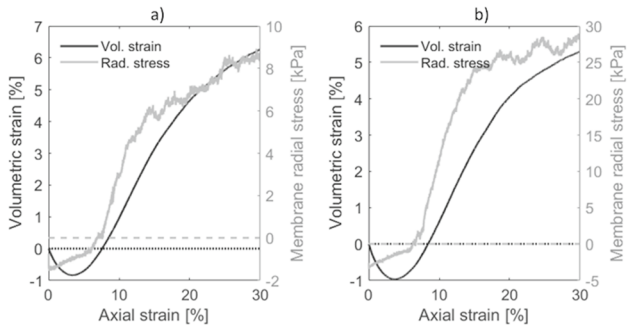


**Fig. 10** Comparison of volumetric strain (black curve, left vertical axis) and membrane radial stress (grey curve, right vertical axis) for two DEM simulations of sand samples using a bonded membrane, respectively at 60 kPa (left) and 300 kPa (right) confining pressure. The dashed lines are the gridlines at zero volumetric strain (black) and zero radial stress (grey)

stress on the volumetric strain instead of radial strain can be explained considering that axial strain affects the ability of the membrane to deform radially. In this particular case, as the sample shortens axially, the membrane becomes less

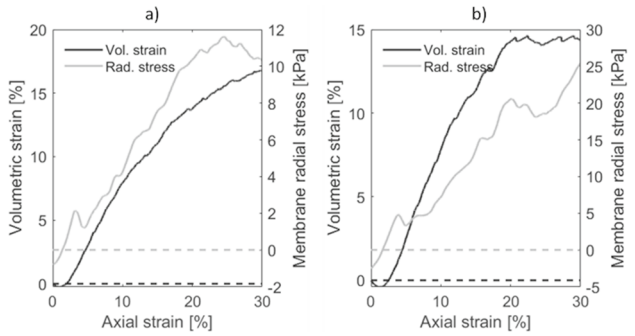


**Fig. 11** Comparison of volumetric strain (black curve, left vertical axis) and membrane radial stress (grey curve, right vertical axis) for two DEM simulations of ballast samples using a faceted membrane, respectively at 60 kPa (left) and 150 kPa (right) confining pressure. The dashed lines are the gridlines at zero volumetric strain (black) and zero radial stress (grey)

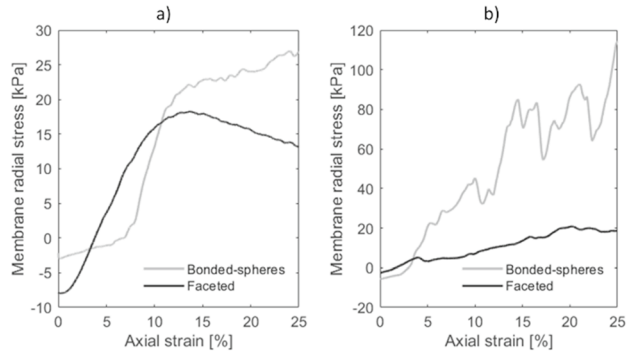


**Fig. 12** Comparison of membrane radial stress calculated for simulations of **a** sand and **b** ballast, at 300 kPa confining pressure, with two different membrane models (bonded spheres and faceted)

constrained, and can therefore more easily deform radially. Figure 11 shows that the same result holds also for a different sample (ballast); data is less smooth because of the small number of grains, but the correlation appears quite clearly, nonetheless.

A comparison of the behaviour of the two membrane models shows similar results from a qualitative point of view for the sand sample, even at relatively large stress levels (Fig. 12a), despite a small softening observed with the faceted membrane. With ballast, on the other hand, the responses of the two models tend to diverge more clearly, especially at large strains (Fig. 12b); in particular, the bonded spheres model shows more scattered data and a much larger increase in radial stress, with no plateau. This might be explained with reference to the particular deformation pattern of this test (high dilation, highly heterogeneous deformation), which may cause unrealistically large bond forces developing locally when neighbouring spheres are pushed away from each other. This is a limitation of the

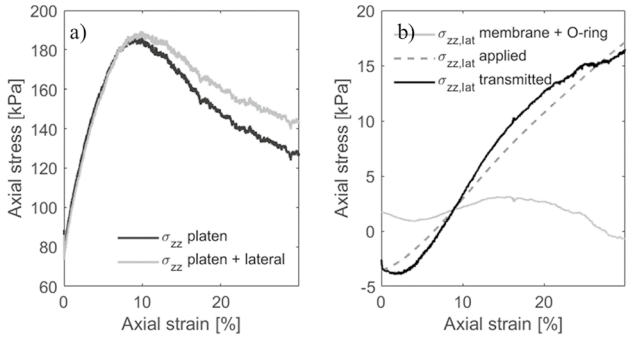


**Fig. 13** **a** Vertical stress from external forces (platen only, and both platen and membrane); **b** vertical stress contributions from membrane and O-rings, and vertical stress applied as part of the confining pressure, from DEM simulation on sand with faceted membrane, under 60 kPa confining pressure

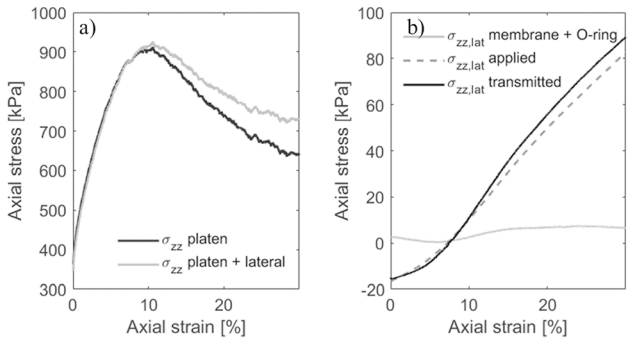


**Fig. 14** **a** Vertical stress from external forces (platen only, and both platen and membrane); **b** vertical stress contributions from membrane and O-rings, and vertical stress applied as part of the confining pressure, from DEM simulation on sand with faceted membrane, under 300 kPa confining pressure

bonded spheres model that should be taken into account. Also, in this situation, the bonded spheres membrane has been found to be likely to fail, with gaps opening and grains free to escape, whereas the faceted one has shown robust behaviour also under large stresses. All this corroborates the preference for a faceted model.

### 4.3 Membrane effect and correction of axial stress

As explained in Sect. 3.4, there are two sources of error that may cause a deviation of the real axial stress from the axial stress that would be measured simply from contacts between end platens and grains. One source is the stress associated with membrane deformation and O-ring connections, in the same way as discussed in Sect. 4.2 for the radial direction. The other source is the vertical component of the confining pressure, which acts perpendicularly to the lateral membrane: as this deforms, it deviates from the right cylinder shape, and therefore a stress component arises in the axial direction (Fig. 5). While this is often overlooked, it can sometimes cause a significant error, that should be taken into account appropriately. Figures 13 and 14 show all these stress components associated with the membrane deformation, for simulations on sand at different stress levels. The sum of membrane and O-ring components is the equivalent, in the axial direction, of the stress component in the radial direction in Fig. 9. The component of axial stress due to the confining pressure is also shown; the sum of these components is equal to the component of stress transmitted to the sample (in the same way as observed in Fig. 9 and demonstrated in Eq. 6). The membrane and O-ring component is found to be small compared to the stress component due to confining pressure, which increases linearly and, at large strain, can be as large as 15% of the total axial stress.

This monotonic increase of membrane axial stress is different from the membrane radial stress, which was found to stabilise at large strains, showing a good correlation with volumetric strain. Axial stress correlates well with radial strain (Fig. 15), as its main effect is a purely geometric one, related with the way the membrane deforms radially. The membrane's deviation from cylindrical shape is clearly correlated with radial strain: as the sample expands radially, the amount of membrane surface with a vector area in the vertical direction also increases. A simple expression for the estimation of the amount of stress applied in the axial direction as effect of the confining pressure can be obtained assuming a linear proportion between the applied stress $\sigma_{zz}^{app,lat}$ and the radial strain. An empirical equation that links these terms through a constant $k = 1.8$ and the cell pressure $p$ was found to give a good approximation of the excess vertical stress due to membrane deformation, with an error $< 1\%$ even at large strains:

$$\sigma_{zz}^{app,lat} = 1.8 p \varepsilon_r. \tag{7}$$

This is found to hold for several different simulations for which the profile of membrane deformation is smooth, and generally characterised by bulging. It is slightly less accurate, but still provides a good estimation, whenever the membrane profile gets very irregular, due to the sample being made of few large particles, as is the case for ballast.

Stress correction in both axial and radial direction was shown to be affected by the radial and volumetric deformation of the sample. To emphasise this, simulations of the same sand sample were carried out with different values of interparticle friction coefficient ($\mu = 0.2$ and an artificially high 0.7, Fig. 16). The higher $\mu$ results in a significantly higher dilation and radial strain. The effect on radial stress (Fig. 16a) and axial stress (Fig. 16b) is an increase of both stress components with respect to the case of $\mu = 0.2$.

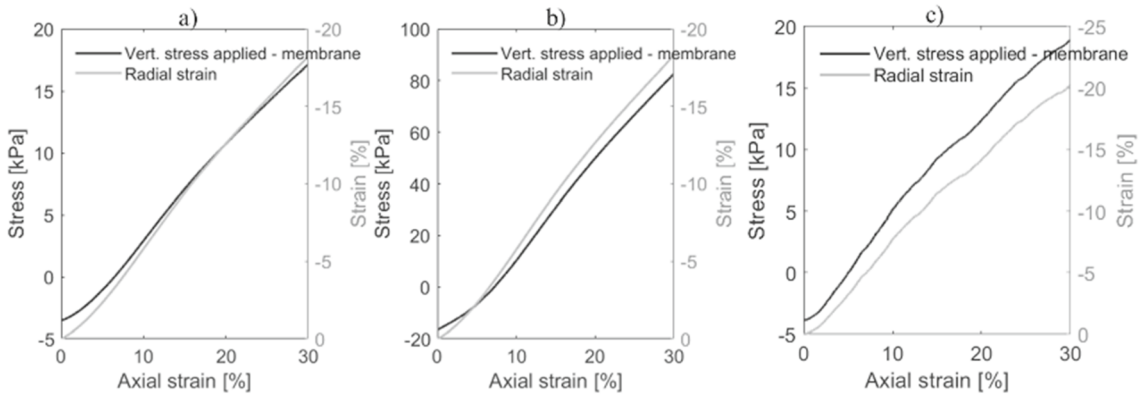


**Fig. 15** Correlation between vertical stress component applied through the membrane (black curve, left vertical axis) and radial strain (grey curve, right vertical axis) for the following DEM simulations: **a** sand, 60 kPa; **b** sand, 300 kPa; **c** ballast, 60 kPa

### 4.4 Stress invariants

It can be useful to analyse these corrections in terms of the stress invariants that are widely used in soil mechanics. At the same time, stress can be calculated in simulations in the same way it is commonly measured in experiments, to compare this with the real stress within the sample that is obtained from contact forces.

Figure 17 compares the deviatoric stress $q$ and mean pressure $p$. Internal stress invariants are obtained from interparticle contact forces, as in Eq. 3. They are calculated as $q = \sigma_{ax} - \sigma_{rad}$ and $p = (\sigma_{ax} + 2\sigma_{rad})/3$; axial and radial stresses are obtained from the stress tensor components as $\sigma_{ax} = \sigma_{zz}$ and $\sigma_{rad} = 0.5(\sigma_{xx} + \sigma_{yy})$. The same invariants are calculated as they would be measured in experiments by taking $\sigma_{ax} = 0.5\left(\sigma_{ax,top} + \sigma_{ax,bot}\right) = 0.5(F_{top} + F_{bot})/A$, where $F_{top}$ and $F_{bot}$ are the total contact forces at the end platens, and $A$ is the average cross-sectional area of the sample. Figure 17a also shows the actual correction $\Delta q = q_{int} - q_{exp}$, as well as the estimated correction based on the formula provided by the specifications: $\Delta q = \frac{4E_m t_m \varepsilon_a}{D_c}$, where $E_m$ and $t_m$ are membrane parameters (Young's modulus and thickness, respectively) as defined in Sect. 4.1, $\varepsilon_a$ is the axial strain and $D_c$ the sample diameter after consolidation [27]. This formula, applied to the case of this DEM model, can underestimate the correction. The specifications only provide a correction for the deviatoric stress, but mean pressure is also subject to error as shown in Fig. 17b. The underestimation of both stress invariants means that the error in terms of dimensionless measures such as stress ratio $q/p$ or mobilised friction angle $\Phi$ is lower, though non-negligible as shown in Fig. 18a, both at peak and at critical state. Looking at the individual stress components in axial and radial direction, it can be observed that the axial stress is consistently smaller than it should be when computed from external (platen) forces, and the radial stress is slightly larger at first, and is then overcome by the real (internal) radial stress which increases as the membrane deforms.

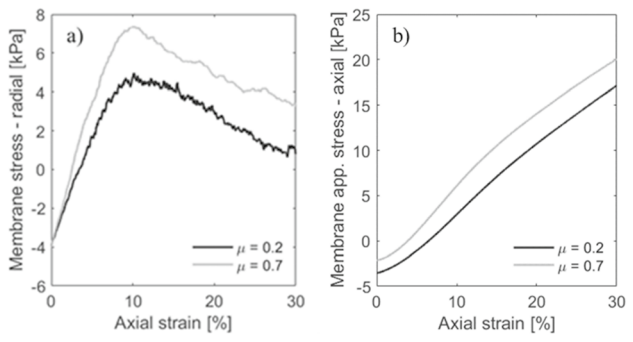


**Fig. 16** Evolution during shearing of **a** membrane radial stress and **b** axial stress applied through the membrane as a function of interparticle friction (different volumetric behaviour)

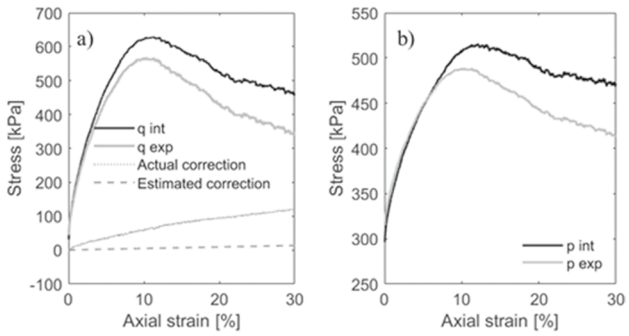


**Fig. 17** **a** Deviatoric stress invariant q and **b** mean pressure p calculated from internal forces and from external forces (as they would be measured in experiments). The actual correction of q (difference between the two curves) and its estimation with the correction provided by the specifications are also shown on the left. Results from simulation of sand with bonded spheres membrane and 300 kPa confining pressure

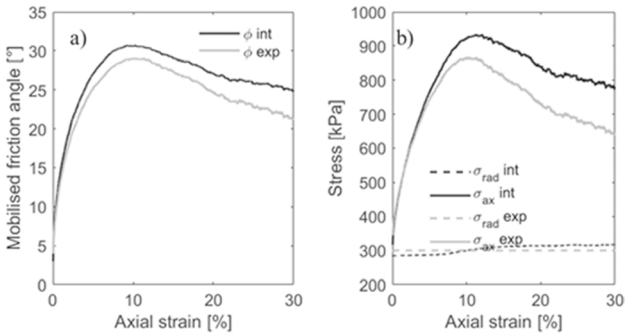


**Fig. 18** **a** Mobilised friction angle Φ and **b** axial and radial stress calculated from internal forces and from external forces (as they would be measured in experiments). Results from simulation of sand with bonded spheres membrane and 300 kPa confining pressure

## 5 Conclusions

A new method for the modelling of a flexible membrane in DEM simulations of triaxial test has been proposed. This method consists in a faceted wall that is used to model the membrane as a continuum. It was shown to perform well after being tested on two different samples: a sample of sand with a relatively large number of grains and a smooth deformation of the membrane, and a sample of railway ballast with few large grains and large pores, with a very irregular membrane deformation. The model was also compared to the well-established bonded spheres membrane, showing that the two methods give similar results. The faceted membrane has some inherent benefits: geometric continuity independently of resolution, which allows for a good response even with a relatively low resolution, which is not the case for the other model; and also permits the possibility of directly taking into account the real material and geometric properties of the membrane. This seems to indicate that the faceted model may in the future substitute the bonded spheres model.

The two models were then used to determine the effect of membrane deformation on the stress within a sample, starting with the definition of stress from single forces derived from the classic Love-Weber formula. Stress tensor contributions were determined for each part of the DEM model, including the membrane and its connections to the end platens. In this way, it was also possible to achieve a better understanding of the origin of the difference between the stress as it is measured in experiments (a constant lateral pressure, and an axial stress coming from forces measured at the end platens) and the real stress within the sample, that can be measured in DEM from contact forces. This consists in an effect in both radial and axial direction. Membrane radial stress was found to be correlated with the volumetric deformation of the sample; it can have a tensile effect (reducing compression) when the sample has contracted, but most importantly it has a compressive effect when it dilates; it was also found to be proportional to the stress level. Axial stress has a similar component due to membrane tension and O-ring connections; however, the most significant error in this direction was found to be related to the vertical component of confining pressure. This is often overlooked as the sample is assumed to undergo a right-cylinder deformation; however, this assumption is in fact quite far from reality, and it can be responsible for a quite large, non-negligible error on the axial stress. It is recommended that this is taken into account appropriately when calculating the stress in a DEM simulation of triaxial test, when this is not done directly from internal contact forces.

Some of these findings shed more light onto the estimation of membrane effect in laboratory triaxial tests, which has been a subject of research in the field of laboratory testing for decades. Membrane effect is shown here to originate from both the tension in the membrane and its curvature. Currently, the standard approach only takes into account the first aspect, neglecting the effect of membrane curvature, i.e. the presence of a vertical component of confining pressure. This additional stress, which can be positive or negative, was found to correlate well with radial strain, therefore an empirical formula for the correction of this component as a function of radial strain has been proposed.

As for the effect of membrane tension, its treatment in the current standards also appears to be incomplete. Currently a correction is applied directly only to the deviatoric stress; it would be better to compute corrections separately for axial and radial stress, and consequently determine a correction also for mean pressure. Furthermore, the empirical formula for deviatoric stress correction only depends on the axial strain, and does not account for the radial or volumetric strain (any two of these will give the third) which have been shown to be directly correlated with the measured membrane stress; in particular, it is important to express membrane correction as a function of the volumetric response of a sample, since the tendency of a sample to dilate affects both membrane tension and its curvature.

**Acknowledgements** This work was supported by the Engineering and Physical Sciences Research Council [grant number EP/W000563/1] in collaboration with Dr. B. A. Baudet and Professor M. R. Coop at University College London.

**Data availability** Data will be made available on request.

## Declarations

**Conflict of interest** The authors declare that they have no known competing financial interests or personal relationships that could have appeared to influence the work reported in this paper.

## References

1. Henkel, D.J., Gilbert, G.D.: The effect of the rubber membrane on the measured triaxial compression strength of clay samples. Géotechnique **3**(1), 20–29 (1952)
2. La Rochelle, P., Leroueil, S., Trak, B., Blais-Leroux, L., Tavenas, F.: Observational approach to membrane and area corrections in triaxial tests. In: Donaghe, R. T., Chaney, R. C., Silver, M. L., Advanced Triaxial Testing of Soil and Rock, pp. 715–731 (1988)
3. Belheine, N., Plassiard, J.P., Donzé, F.V., Darve, F., Seridi, A.: Numerical simulation of drained triaxial test using 3D discrete element modeling. Comput. Geotech. **36**(1–2), 320–331 (2009)
4. Salot, C., Gotteland, P., Villard, P.: Influence of relative density on granular materials behavior: DEM simulations of triaxial tests. Granul. Matter **11**(4), 221–236 (2009)
5. Cheung, G., O'Sullivan, C.: Effective simulation of flexible lateral boundaries in two- and three-dimensional DEM simulations. Particuology **6**(6), 483–500 (2008)
6. Kawamoto, R., Andò, E., Viggiani, G., Andrade, J.E.: All you need is shape: Predicting shear banding in sand with LS-DEM. J. Mech. Phys. Solids **111**, 375–392 (2018)
7. Zhang, J., Wang, X., Yin, Z.Y., Liang, Z.: DEM modeling of large-scale triaxial test of rock clasts considering realistic particle shapes and flexible membrane boundary. Eng. Geol. **279**(October), 105871 (2020)
8. de Bono, J., McDowell, G.R., Wanatowski, D.: Discrete element modelling of a flexible membrane for triaxial testing of granular material at high pressures. Geotech. Lett. **2**(4–6), 199–203 (2012)
9. Cil, M.B., Alshibli, K.A.: 3D analysis of kinematic behavior of granular materials in triaxial testing using DEM with flexible membrane boundary. Acta Geotech. **9**(2), 287–298 (2014)
10. de Bono, J., McDowell, G.R.: Micro mechanics of drained and undrained shearing of compacted and overconsolidated crushable sand. Geotechnique **68**(7), 575–589 (2018)
11. de Bono, J., McDowell, G.R.: On the packing and crushing of granular materials. Int. J. Solids Struct. **187**, 133–140 (2020)
12. Tolomeo, M., McDowell, G.R.: DEM study of an 'avatar' railway ballast with real particle shape, fabric and contact mechanics. Granul. Matter **25**(2), 1–13 (2023)
13. PFC—Particle Flow Code, Ver. 7.0. Itasca Consulting Group, Inc., Minneapolis: Itasca (2021)
14. FLAC3D—Fast Lagrangian Analysis of Continua in Three-Dimensions, Ver. 7.0. Itasca Consulting Group, Inc., Minneapolis: Itasca (2019)
15. Qin, Y., et al.: A three-dimensional discrete element model of triaxial tests based on a new flexible membrane boundary. Sci. Rep. **11**(1), 1–13 (2021)
16. Qu, T., Feng, Y.T., Wang, Y., Wang, M.: Discrete element modelling of flexible membrane boundaries for triaxial tests. Comput. Geotech.. Geotech. **115**(June), 103154 (2019)
17. Huang, S., Qian, Y., Shan, Y.: Effect of flexible membrane in large-scale triaxial test DEM simulations. Constr. Build. Mater. **370**(October), 130608 (2023)
18. Le Pen, L., Harkness, J., Zervos, A., Powrie, W.: The influence of membranes on tests of coarse-grained materials at low cell pressures. In: Geomechanics from Micro to Macro—Proceedings of TC105 ISSMGE International Symposium on Geomechanics from Micro to Macro, IS-Cambridge 2014, vol. 1, pp. 449–454 (2015)
19. Nicot, F., Hadda, N., Guessasma, M., Fortin, J., Millet, O.: On the definition of the stress tensor in granular media. Int. J. Solids Struct. **50**(14–15), 2508–2517 (2013)
20. Love, A.E.H.: A Treatise of Mathematical Theory of Elasticity. Cambridge University Press, Cambridge (1927)
21. Weber, J.: Recherches concernant les contraintes intergranulaires dans les milieux pulvérulents. Bull. Liaison Ponts Chaussées **20**, 3.1-3.20 (1966)
22. Christoffersen, J., Mehrabadi, M.M., Nemat-Nasser, S.: A micromechanical description of granular material behavior. J. Appl. Mech. **48**(2), 339 (1981)
23. Midi, G.: On dense granular flows. Eur. Phys. J. E **14**(4), 341–365 (2004)
24. Tolomeo, M., McDowell, G.R.: Modelling real particle shape in DEM: a comparison of two methods with application to railway ballast. Int. J. Rock Mech. Min. Sci. **159**, 105221 (2022)
25. Wong, C.P.Y., Coop, M.R.: Development of inter-particle friction in a railway ballast. Geotech. Lett. **10**(4), 535–541 (2020)
26. Nardelli, V., Coop, M.R.: The experimental contact behaviour of natural sands: normal and tangential loading. Geotechnique **69**(8), 672–686 (2019)
27. ASTM D7181: Standard Test Method for Consolidated Drained Triaxial Compression Test for Soils, p. 12. ASTM International (2011)